Received: 6 June 2023 | Revised: 10 November 2023 | Accepted: 4 December 2023

DOI: 10.1002/pro.4854

RESEARCH ARTICLE

THE PROTEIN SOCIETY WILEY

Human islet amyloid polypeptide-induced β-cell cytotoxicity is linked to formation of α-sheet structure

Cheng-Chieh Hsu[1,2] | **Andrew T. Templin**[3] | **Tatum Prosswimmer**[2] | **Dylan Shea**[2] | **Jinzheng Li**[4] | **Barbara Brooks-Worrell**[3] | **Steven E. Kahn**[3] | **Valerie Daggett**[1,2,4]

[1]Department of Bioengineering, University of Washington, Seattle, Washington, USA

[2]Molecular Engineering Program, University of Washington, Seattle, Washington, USA

[3]Division of Metabolism, Endocrinology and Nutrition, Department of Medicine, VA Puget Sound Health Care System and University of Washington, Seattle, Washington, USA

[4]Department of Biochemistry, University of Washington, Seattle, Washington, USA

Correspondence
Valerie Daggett, Department of Bioengineering, University of Washington, Seattle, WA 98195-5013, USA.
Email: daggett@uw.edu

Steven E. Kahn, Division of Metabolism, Endocrinology and Nutrition, Department of Medicine, VA Puget Sound Health Care System and University of Washington, Seattle, WA 98108, USA.
Email: skahn@uw.edu

Funding information
American Diabetes Association; National Institutes of Health, Grant/Award Numbers: GMS 95808, F32-DK-107022, P30-DK-017047; U.S. Department of Veterans Affairs; University of Washington Office of Research and Department of Bioengineering; Diabetes Research Center at the University of Washington; UW Mary Gates Research Scholarship; National Institute of Health Bioengineering and Cardiovascular Training Grant; Molecular Biophysics Training Grant

Review Editor: Jean Baum

Abstract

Type 2 diabetes (T2D) results from insulin secretory dysfunction arising in part from the loss of pancreatic islet β-cells. Several factors contribute to β-cell loss, including islet amyloid formation, which is observed in over 90% of individuals with T2D. The amyloid is comprised of human islet amyloid polypeptide (hIAPP). Here we provide evidence that early in aggregation, hIAPP forms toxic oligomers prior to formation of amyloid fibrils. The toxic oligomers contain α-sheet secondary structure, a nonstandard secondary structure associated with toxic oligomers in other amyloid diseases. De novo, synthetic α-sheet compounds designed to be nontoxic and complementary to the α-sheet structure in the toxic oligomers inhibit hIAPP aggregation and neutralize oligomer-mediated cytotoxicity in cell-based assays. In vivo administration of an α-sheet design to mice for 4 weeks revealed no evidence of toxicity nor did it elicit an immune response. Furthermore, the α-sheet designs reduced endogenous islet amyloid formation and mitigation of amyloid-associated β-cell loss in cultured islets isolated from an hIAPP transgenic mouse model of islet amyloidosis. Characterization of the involvement of α-sheet in early aggregation of hIAPP and oligomer toxicity contributes to elucidation of the molecular mechanisms underlying amyloid-associated β-cell loss.

KEYWORDS

α-sheet, islet amyloid, islet amyloid polypeptide, toxic soluble oligomers, type 2 diabetes

Cheng-Chieh Hsu and Andrew T. Templin contributed equally.

1 | INTRODUCTION

An estimated 537 million people have diabetes worldwide and this number is expected to increase to over 783 million by 2045, with ≥90% of the cases being type 2 diabetes (T2D) (Saeedi et al., 2019). T2D is associated with pancreatic islet β-cell dysfunction and death, resulting in insufficient insulin secretion and the development of hyperglycemia (Kahn et al., 2006). Numerous factors, including free fatty acids, proinflammatory cytokines, and islet amyloid formation, may cause T2D (Cnop et al., 2005; Federici et al., 2001; Hull et al., 2004; Kharroubi et al., 2004). Progressive loss of β-cell function is central to the development and progression of T2D (Cnop et al., 2007). Existing glucose-lowering medications are unable to maintain adequate glucose control, resulting in numerous secondary complications caused by glycemic damage (Forbes & Cooper, 2013).

Islet amyloid deposits, comprised of aggregated islet amyloid polypeptide (IAPP), are observed in over 90% of individuals with T2D (Cooper et al., 1987; Hull et al., 2004; Westermark et al., 1987). IAPP is a 37-residue peptide hormone that is synthesized in β-cells and is co-secreted with insulin (Kahn et al., 1990). Unlike IAPP in species such as mice and rats, human IAPP is amyloidogenic and forms fibrillar amyloid deposits (Betsholtz et al., 1989; Cao et al., 2010). The presence of cytotoxic hIAPP is involved in the development of diabetic phenotypes in a humanized mouse model (Kim et al., 2021). hIAPP is intrinsically disordered; however, under amyloidogenic conditions, it aggregates to form a heterogeneous distribution of soluble oligomers prior to forming insoluble, mature fibrils (Butler et al., 2003; Cooper et al., 1987; Meier et al., 2006; Ritzel et al., 2007; Shigihara et al., 2014; Westermark et al., 1987; Zraika et al., 2010). The soluble oligomeric forms of hIAPP are cytotoxic and are responsible for β-cell death (Meier et al., 2006). Compounds that target mature amyloid fibrils can inhibit further fibril formation, but they do not prevent β-cell death, (Meier et al., 2006), nor, necessarily, result in reduced cell death, further supporting the toxic oligomer hypothesis (Oskarsson et al., 2018).

Since the hIAPP monomer is the biologically functional form and its mature fibrils are nontoxic, selective targeting of cytotoxic hIAPP oligomers may represent a new approach to development of T2D treatments. It has been suggested that amyloidogenic toxic oligomers contain a common structure and mechanism of toxicity (Bucciantini et al., 2002; Kayed et al., 2003). Although the molecular mechanism of hIAPP aggregation in the pathogenesis of T2D is not entirely clear, hIAPP is believed to adopt a nonstandard secondary structure during aggregation and oligomer formation, as has been observed in other amyloidogenic proteins. We hypothesized that α-sheet (Armen, Alonso, & Daggett, 2004; Daggett, 2006; Hopping et al., 2014; Kellock et al., 2016; Maris et al., 2018) forms in the toxic oligomers during the early stages of hIAPP aggregation. This hypothesis arose from our observation that α-sheet structure forms in molecular dynamics (MD) simulations of multiple amyloidogenic peptides and proteins under amyloidogenic conditions, but not native conditions (Armen, Alonso, & Daggett, 2004; Armen, DeMarco, et al., 2004; Daggett, 2006). α-Sheet is defined by the alignment of the amide groups on one side of the backbone and the carbonyl groups on the other (Daggett, 2006). We designed nontoxic, stable α-sheet peptides complementary to the presumed α-sheet structure in the toxic oligomers (Bleem et al., 2017; Bleem et al., 2023; Daggett, 2006; Hopping et al., 2014; Kellock et al., 2016; Maris et al., 2018; Prosswimmer & Daggett, 2022; Shea et al., 2019). We reasoned that these α-sheet peptides would neutralize toxicity and inhibit fibril formation by specifically binding to toxic oligomers.

Here we present experimental results demonstrating that hIAPP oligomers adopt α-sheet structure and that de novo designed α-sheet compounds inhibit toxicity and fibrillization both in a β-cell line-based assay and in cultured transgenic mouse islets that express hIAPP and develop islet amyloid. In addition, in vivo dosing of mice with a designed α-sheet compound showed no evidence of toxicity and did not elicit an immune response to the α-sheet peptide.

2 | RESULTS

2.1 | Establishing the timeline of hIAPP aggregation kinetics in vitro

hIAPP aggregation was monitored with thioflavin T (ThT) under different solvent conditions, peptide concentrations, and mechanical agitation. As hIAPP readily aggregates and sticks to surfaces, organic solvents, such as HFIP and DMSO, are routinely used followed by dilution with buffer (Brender et al., 2015; Butler et al., 2003; Cao et al., 2013; De Carufel et al., 2013; Kellock et al., 2016; Oskarsson et al., 2018) or DMSO-free Tris buffer (Abedini et al., 2016; De Carufel et al., 2013; Sebastiao et al., 2017). We tested commonly employed buffers and conditions and observed sigmoidal kinetics indicative of a nucleation polymerization pathway (Linse, 2017), but the kinetics varied under the different conditions (Figure S1). For example, 25 μM hIAPP in DMSO/PBS and in Tris–HCl showed similar aggregation behavior, but with

different onset of exponential fluorescence (Figure S1A). As organic solvents can present difficulties with other employed methodologies, we developed and proceeded with an ice-cold PBS method. In addition, we also lowered the concentration of hIAPP from 25 to 15 μM to prolong the lag period (Figure 1a).

2.2 | hIAPP forms α-sheet secondary structure and is cytotoxic early in amyloidogenesis

The undisturbed ice-cold PBS ThT time course in Figure 1a was used to determine pre-incubation times to evaluate structure during aggregation using CD spectroscopy. Monomeric hIAPP was largely unstructured (Figure 1b). The spectra lifted as aggregation proceeded and exhibited a "null" signal at 3.5 h, as expected for α-sheet (Bleem et al., 2017; Hopping et al., 2014; Kellock et al., 2016; Maris et al., 2018; Shea et al., 2019). The curve then pulled downward during the sigmoidal portion of the corresponding ThT curve and adopted the characteristic spectrum for β-sheet structure in the plateau region (Figure 1b). In contrast, rat IAPP (rIAPP) did not undergo structural changes (Figure 1a,c). A representative curve for an α-sheet hairpin, AP407, and its NMR structure (Shea et al., 2019), are provided for reference. Cell viability assays were performed using β-and neuronal cells to investigate the toxicity of hIAPP during aggregation (Figure 1d). The toxicity peaked in the lag phase corresponding to α-sheet formation, and dropped when β-sheet protofibrils and fibrils formed.

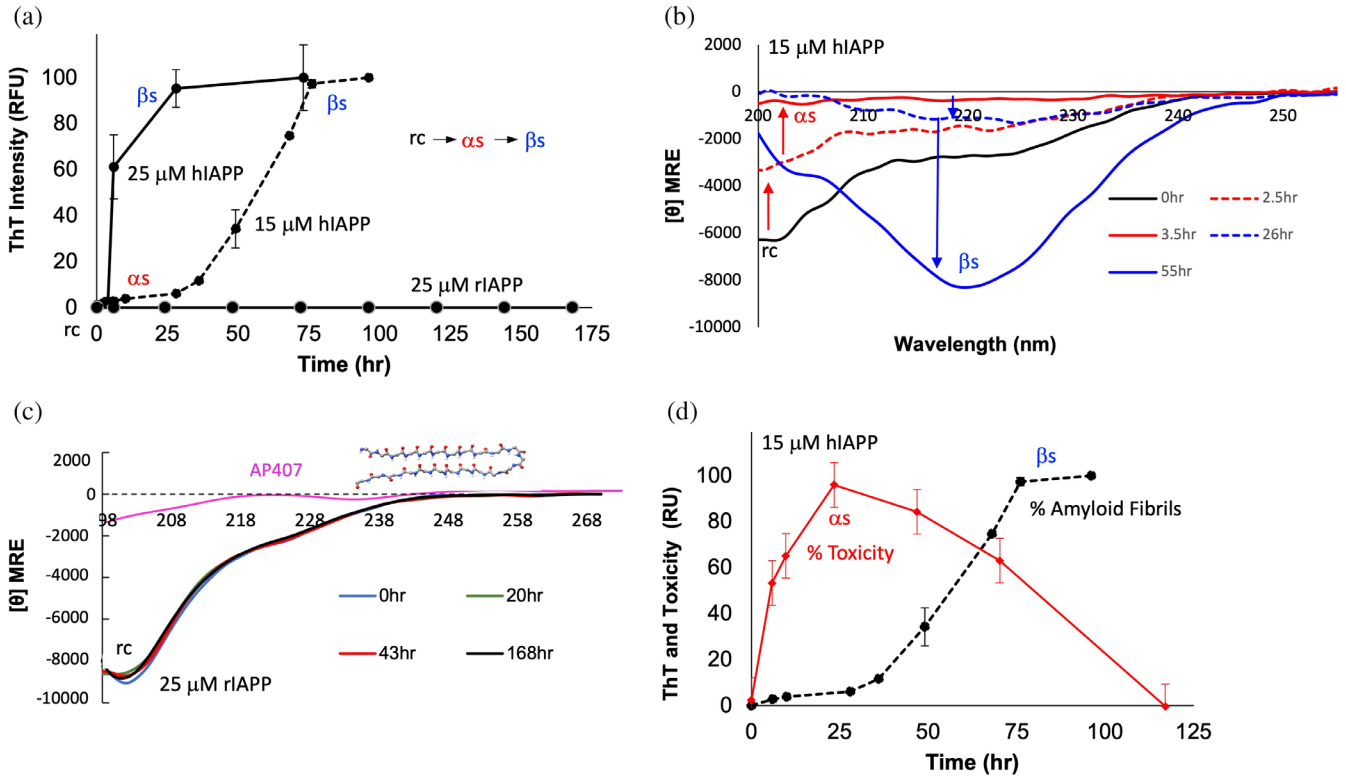

FIGURE 1 Characterization of α-sheet involvement in aggregation. (a) PBS-treated amyloidogenic human IAPP (hIAPP) samples were monitored with undisturbed endpoint measurements at two different concentrations (15 and 25 μM) at 25°C. PBS-treated rodent IAPP (rIAPP; 25 μM) was included as a non-amyloidogenic control. hIAPP followed the same process of conformational conversion at both concentrations, but the kinetics were faster at the higher concentration. rIAPP did not exhibit conformational conversion. Each time point measurement represents mean and standard deviation. $N = 3$ per condition. (b) Circular dichroism spectroscopy analysis of PBS-treated 15 μM hIAPP sampled at different times during aggregation. Spectra for 0 h incubation hIAPP (black) are consistent with a disordered, random coil conformation for the native monomeric state. 2.5 h (red, dotted) and 3.5 h (red, solid) incubation times result in a lift of the curves to essentially featureless "null" spectra. Additional incubation produces a drop near 218 nm consistent with β-sheet structure. (c) CD spectra of 15 μM rIAPP as a function of time, overlaid spectra with different colors that remain random coil over time. The spectrum for the α-sheet AP407 model compound (magenta) is provided for comparison along with its NMR structure. (d) Toxicity time-course of hIAPP. MTT cell viability assay of INS-1 pancreatic β-cells exposed to pre-incubated hIAPP from different incubation duration (15 μM in PBS at 25°C diluted to 5 μM for application to cells). Toxicity is normalized, the maximum toxicity point corresponded to 60% cell viability. $N = 2$–6 per timepoint. The following abbreviations are used in the figure: rc = random coil; αs = α-sheet; βs = β-sheet.

2.3 | Inhibition of hIAPP aggregation and toxicity by designed α-sheet peptides

Given the correlation between α-sheet and toxicity, we tested two α-sheet designs for their ability to inhibit aggregation of hIAPP: our benchmark AP90 sequence and AP5 (a scrambled version of AP90, Table S1). Inhibition was assessed using the undisturbed endpoint ThT method, where excess AP5 and AP90 peptides were incubated with hIAPP at 25°C for 68 h to reach the plateau of the ThT curve (1:4, 25 μM hIAPP:100 μM AP design) (Figure 2a). α-Sheet peptides significantly reduced fibril content, resulting in 88% and 71% inhibition for AP5 and AP90, respectively. P1, a random coil control peptide, had no effect. An MTT cell viability assay was used as a surrogate for toxicity using two cell lines. Pre-incubated hIAPP samples with and without the addition of AP5 were evaluated in INS-1 β-cells and SH-SY5Y neuroblastomas (Figure 2b,c; INS-1 cells: 15 μM hIAPP incubated for 24 and 48 h; SH-SY5Y: 50 μM hIAPP incubated 1.5 h). Addition of AP5 neutralized toxicity in both cell lines, with an increase of 42% and 34% in cell viability at 24 and 48 h (to 100% and 97%, respectively) in the INS-1 β-cells (Figure 2b) and from 11% to 83% for the SH-SY5Y neuroblastoma cells (Figure 2c).

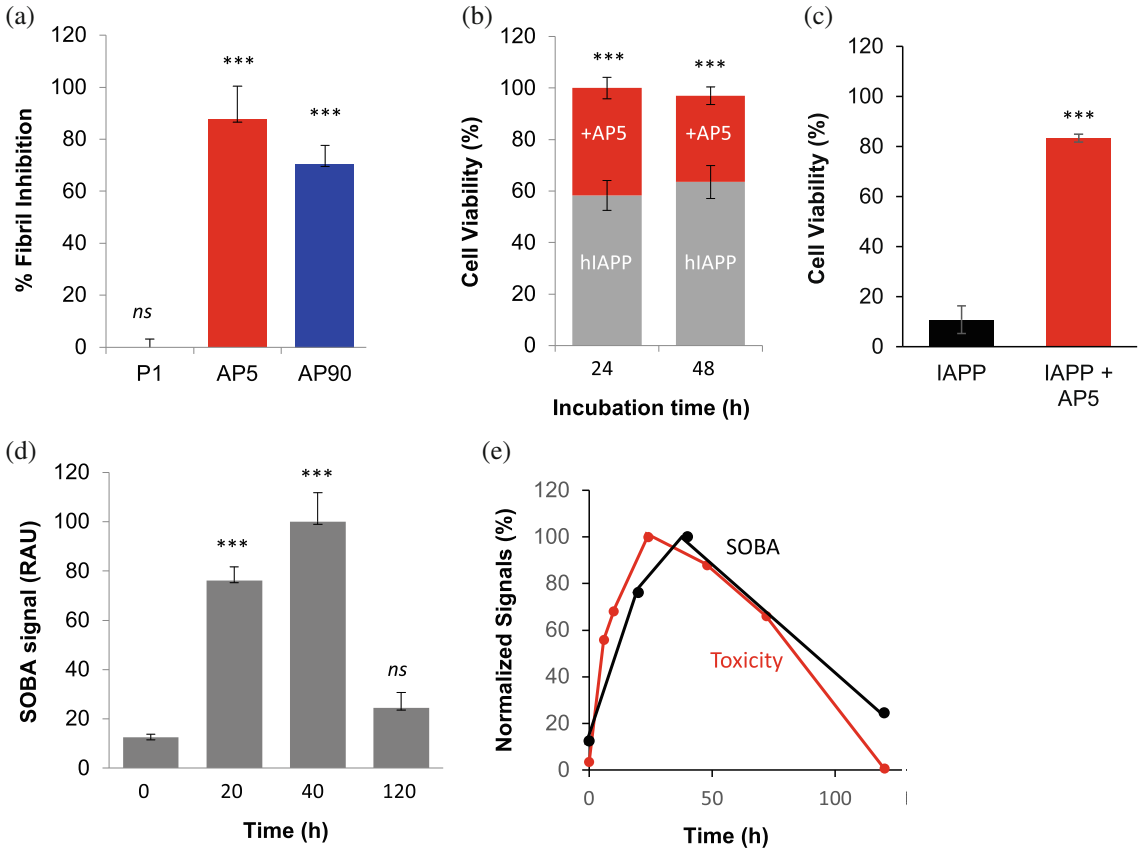

FIGURE 2 Binding of α-sheet peptides to hIAPP. (a) Inhibition of hIAPP aggregation by AP5 and AP90 and lack of inhibition with the P1 peptide. Designed peptides were co-incubated with hIAPP at 1:4 molar ratio (hIAPP: AP peptide). Data bars represent standard deviation. $N = 8$ for hIAPP, AP5, and AP90 conditions. $N = 3$ for P1. For all panels, $^{*}p < 0.05$, $^{**}p > 0.01$, $^{***}p < 0.001$, $ns \geq 0.05$, and error bars represent standard deviations. (b) Insulinoma cell viability when incubated with hIAPP in the absence of AP5 (gray) and in the presence of AP5 (red). AP5 significantly neutralized the toxicity of oligomeric hIAPP (2.5:1 molar ratio, 37.5 μM AP5 and 15 μM IAPP) preincubated for 24 ($p = 0.0006$) and 48 ($p = 0.004$) hours (p-values relative to untreated hIAPP). Vertical bars represent standard deviation. $N = 3$–6 per condition. (c) SH-SY5Y neuroblastoma cell viability when incubated with hIAPP in the absence of AP5 (black) and the presence of AP5 (red). Oligomeric IAPP (50 μM, 1.5 h preincubation, corresponding to formation of α-sheet oligomers at this high concentration) reduced cell viability ($p = 0.0002$ relative to medium with vehicle), and the addition of AP5 (1:1 molar ratio) resulted in significant recovery of cell viability ($p = 0.0004$, relative to untreated hIAPP). Vertical bars represent standard deviation. $N = 3$ per condition. (d) The soluble oligomer binding assay of hIAPP sampled at different times during aggregation. The hIAPP samples (15 μM) were incubated and then diluted to 5 μM immediately before the assay. Higher absorbance values denote higher amounts of hIAPP α-sheet oligomers. hIAPP at 20 h ($p = 0.0002$) and 40 h ($p = 0.0007$) showed significant binding compared to 0 h. Vertical bars represent standard deviation. $N = 4$ per condition. $^{***}p < 0.001$ vs. 0-h sample. (e) Binding of hIAPP α-sheet oligomers in the SOBA assay is correlated with toxicity (given as the inverse of the cell viability).

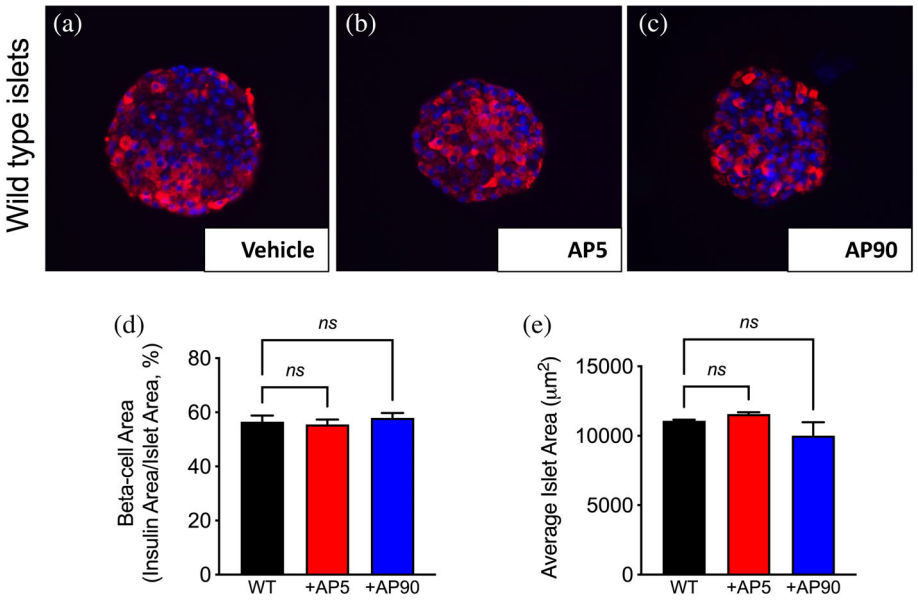

FIGURE 3 Histological examination of wild-type mouse islets co-incubated without or with α-sheet peptides. Representative images of wild type mouse islets treated with (a) vehicle, (b) 100 μM AP5 or (c) 100 μM AP90. Blue staining represents cell nuclei and red staining represents insulin. (d) β-cell area (insulin area/islet area, %) and (e) islet area (mm^2) were quantified from wild-type mouse islets treated without or with α-sheet peptides. Vertical bars represent standard error of the mean. $N = 3$ per condition. *ns* $p > 0.05$ vs. untreated islets.

2.4 | Specific binding of α-sheet peptides to toxic conformers

The α-sheet structure adopted during the aggregation lag phase was well correlated with cytotoxicity, and α-sheet peptides inhibited hIAPP aggregation and toxicity. To further explore the hIAPP toxic species, we tested the binding of various pre-incubated samples in our Soluble Oligomer Binding Assay (SOBA) (Shea et al., 2019, 2022). SOBA is an ELISA-like assay that uses an α-sheet peptide as the capture agent and provides a readout of α-sheet structure.

hIAPP samples were incubated corresponding to the 15 μM undisturbed ThT curve. Samples pre-incubated for 24 and 48 h displayed higher SOBA signals than the fibril sample (120 h) (Figure 2d). Thus, the binding of hIAPP in the SOBA assay occurred during the lag phase and corresponded to the formation of α-sheet by CD. In contrast, the starting structure (random coil by CD) and the aggregated species (β-sheet by CD) had low SOBA signals. The SOBA signal and toxicity were highly correlated (Figure 2e, $R^2 = 0.97$), supporting the connection between α-sheet and toxicity.

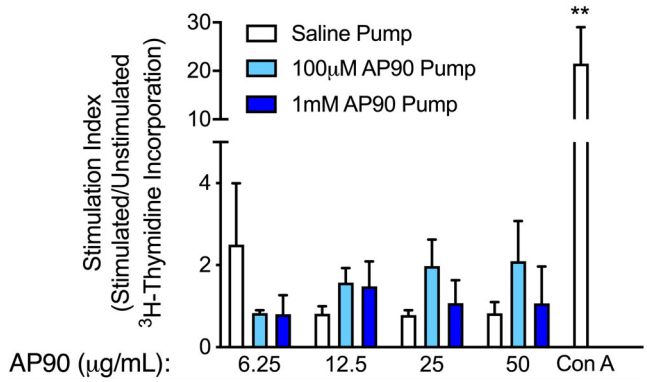

FIGURE 4 Immune response to AP90 after in vivo peptide administration. Following in vivo administration of saline (white bars), 100 μM AP90 (light blue bars), or 1 mM AP90 (dark blue bars) to mice for 4 weeks, peripheral blood mononuclear cells were isolated from spleens and incubated alone (unstimulated), with AP90 (stimulated, 6.25, 12.5, 25, or 50 μg/mL), or with concanavalin A (Con A, 10 μg/mL). Unstimulated and stimulated 18 h-^{3}H-thymidine incorporation was determined by scintillation counting. Stimulation index (SI) was calculated as mean counts per minute (CPM) stimulated/unstimulated. Vertical bars represent standard error of the mean. $^{**}p < 0.01$ vs. all other groups.

2.5 | α-Sheet designs are nontoxic and do not elicit an immune response in vivo

We also evaluated the effect of our α-sheet designs in primary wild-type (WT) mouse islets. Islets were isolated and cultured in the presence or absence of α-sheet designs for 144 h and islet morphology was assessed by quantitative microscopy. In these studies, α-sheet designs were added to cultures of WT mouse islets that express non-amyloidogenic rIAPP to evaluate potential toxicity and side effects. Insulin and islet area were quantified from islet micrographs. Vehicle, AP5, and AP90 treated islets were morphologically very similar (Figure 3a–c), with β-cell and islet area remaining unchanged following treatment with α-sheet compounds (Figure 3d,e).

In vivo tests designed to probe whether α-sheet designs are toxic or immunogenic in live mice were addressed by administering AP90. We implanted peptide-eluting mini-pumps subcutaneously for continuous

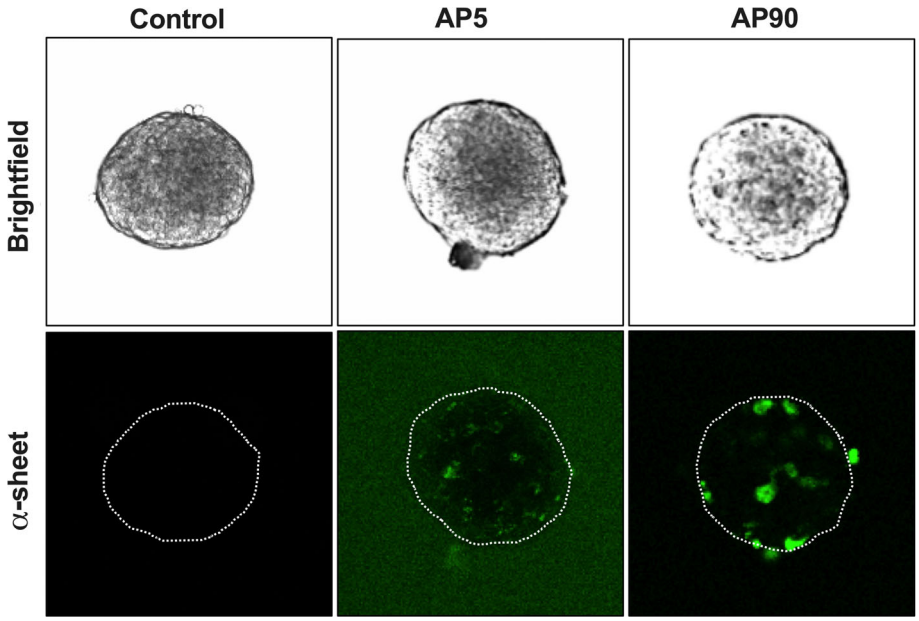

FIGURE 5 Access of amyloid-inhibiting peptides to the intra-islet space. Amyloid-prone hIAPP transgenic islets were cultured in the absence (left) or presence of 100 μM fluorescein labeled AP5 (center) or AP90 (right) peptide. Following 48 h of culture under these conditions, islets were transferred to media lacking peptide and subjected to brightfield (top) and confocal (bottom) microscopy (Leica SP5, 10× magnification). Fluorescein-labeled peptides were imaged by excitation at 488 nm.

administration over 4 weeks. Mice received mini-pumps that eluted either saline, 100 μM AP90 (total dose 0.09 mg/kg body weight), or 1 mM AP90 (total dose 0.9 mg/kg body weight). Mice were evaluated daily and showed no signs of sickness due to peptide infusion or mini-pump implantation surgery. Splenocytes and blood plasma were isolated from the mice following the 4-week dosing regimen, and the presence of AP90 in the plasma was confirmed by mass spectrometry (Figure S3). Splenocytes from mice that received saline or AP90 were tested for immunogenicity against AP90. AP90 failed to stimulate proliferation from any treatment group at concentrations ranging from 6.25 to 50 μg/mL. In contrast, concanavalin A (Con A), a known immune cell mitogen, significantly increased splenocyte proliferation at 10 μg/mL (Figure 4).

2.6 | α-Sheet designs decrease endogenous amyloid formation in isolated islets

Prior to our studies on the effects of α-sheet peptides on islet amyloid formation, we exposed cultured islets to fluorescein-labeled AP5 and AP90 peptides to examine penetrance of the peptides into hIAPP transgenic mouse islets (Figure 5). AP90 was used for further studies to assess the inhibition of endogenous islet amyloid formation because of improved penetrance. Treatment of hIAPP transgenic mouse islets with 100 μM AP90 reduced islet amyloid deposition (thioflavin S, green) and increased β-cell area (insulin, red) (Figure 6a). The reduction was quantified, confirming that AP90 reduced amyloid prevalence (the percentage of islets with amyloid) relative to untreated islets (61.0 ± 9.7% vs. 80.3 ± 6.3% amyloid positive islets, $p = 0.03$, Figure 6b). AP90 also reduced amyloid severity (the percentage of islet area occupied by amyloid) by approximately 60% (2.0 ± 1.0% vs. 5.3 ± 1.9% of islet area, $p = 0.03$, Figure 6c). Importantly, the reduction in islet amyloid observed in hIAPP transgenic islets treated with AP90 was associated with an increase in insulin-positive islet area (57.4 ± 2.6% vs. 49.9 ± 1.9% of islet area, $p < 0.01$, Figure 6d), indicating a reduction in amyloid-associated β-cell loss. The average islet area remained unchanged in the presence of AP90 (*ns*, not statistically significant, $p > 0.05$, Figure 6e).

3 | DISCUSSION

Islet amyloid deposits are associated with the development of diabetic phenotypes (Kim et al., 2021), but the underlying molecular mechanism(s) remains elusive. As mentioned above, organic solvents such as HFIP and DMSO are routinely used to treat hIAPP. The use of these solvents can affect the aggregation kinetics as well as complicate downstream analyses. DMSO is toxic to cells, obscures the far UV region of CD spectra, and prevents accurate determination of hIAPP concentration by UV/Vis spectroscopy. HFIP, like other fluorinated and non-fluorinated alcohols (i.e., Tris), promotes and stabilizes α-helical structure, which can alter the conformational equilibria and affect the kinetics of aggregation (Bleem et al., 2017; De Carufel et al., 2013). Consequently, we developed a protocol to dissolve hIAPP directly into ice-cold PBS buffer, eliminating the need for

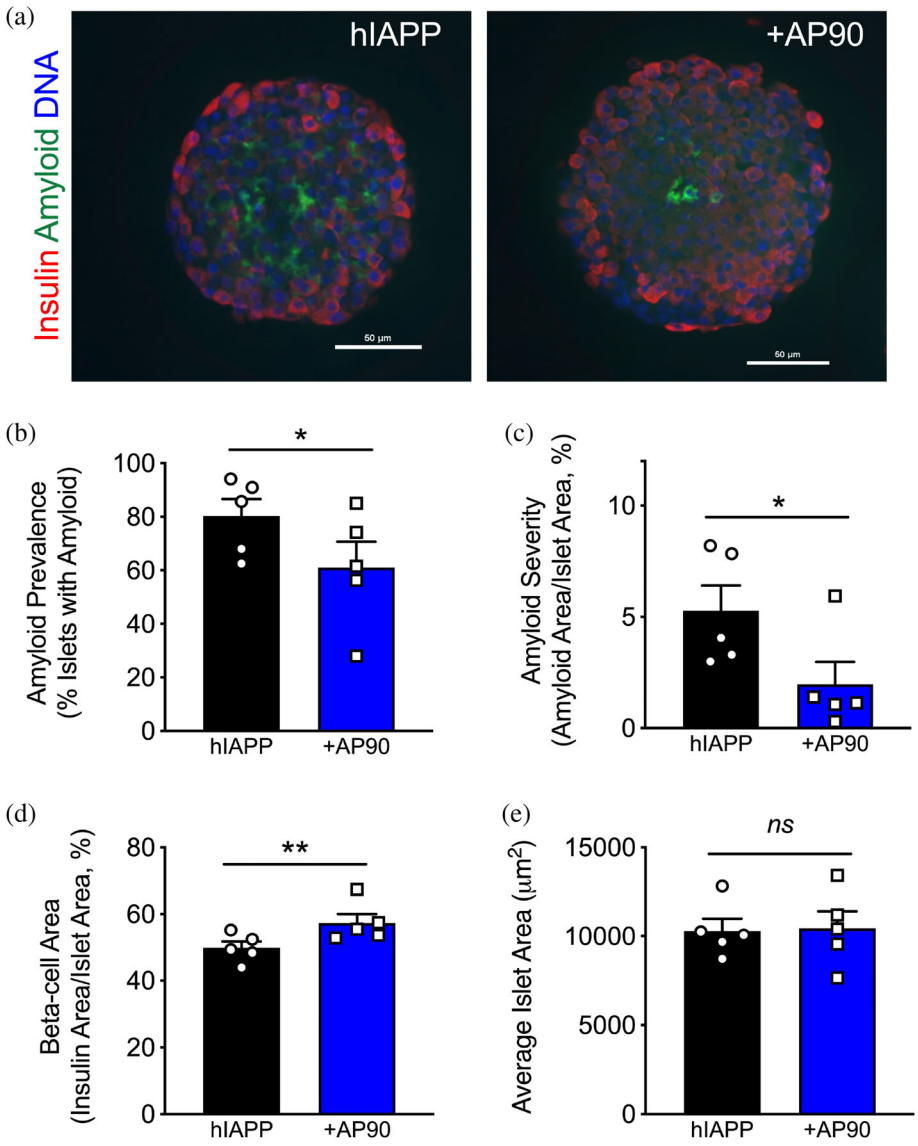

FIGURE 6 Histological examination of hIAPP transgenic mouse islets expressing hIAPP co-incubated with or without α-sheet peptides. Amyloid-prone hIAPP transgenic mouse islets were cultured in 16.7 mM glucose (an amyloidogenic condition) without (hIAPP) or with 100 µM AP90 (+AP90) for 144 h. (a) Representative images of hIAPP transgenic mouse islets with and without AP90 treatment. Blue staining represents cell nuclei, green amyloid deposits, and red insulin. Islets were subjected to quantitative microscopy for determination of (b) amyloid prevalence (% amyloid positive islets), (c) amyloid severity (amyloid area/islet area, %), (d) β-cell area (insulin area/islet area, %), and (e) islet area (mm^2). Vertical bars represent standard error of the mean. $N = 5$ per condition. *$p < 0.05$ or **$p < 0.01$ or *ns* $p > 0.05$ vs. untreated islets.

organic solvents. This solubilization protocol provided the expected sigmoidal kinetics, but in a more physiologically relevant buffer (Figure S1A).

In addition to buffers and co-solvents, the aggregation of hIAPP is very sensitive to environmental conditions, including temperature (Brender et al., 2015), and agitation (Sebastiao et al., 2017). As hIAPP aggregation kinetics provide the timeline for linking different biophysical and biological experiments, ThT monitoring that does not perturb the kinetics is required. Aggregation is typically tracked using continuous or frequent measurements of fluorescence in a plate reader. Using this method, the samples are unintentionally agitated due to the robotic motion of the plate reader during measurement (Sebastiao et al., 2017). This results in artificially faster aggregation kinetics than for individual measurements of undisturbed samples at various points in the aggregation process. As this agitation affects the kinetics, the continuously monitored kinetics of a given sample will not necessarily align with the incubation times used for other biophysical and biochemical characterizations. To illustrate this, the aggregation kinetics of hIAPP were monitored using the continuous and 'undisturbed' methods with our ice-cold PBS protocol (Figure S1B). In the case of 15 µM hIAPP in PBS, the lag phase increased from 8 h to 58 h using the "undisturbed" method relative to the continuous method with readings taken every 10 minutes (Figure S1B), and this effect was independent of solvent (Figure S1C). As hIAPP solubilized with ice-cold PBS displayed behavior consistent with earlier observations, without confounding spectroscopic studies and cell assays, in vitro studies were performed with these conditions to allow experimental coordination based on a reliable aggregation profile (Figure S1A). The "undisturbed" approach mirrors the sample handling for other experiments, such that samples were incubated and

aliquots were removed to link the results of ThT, MTT, and CD experiments. As a control for the behavior of hIAPP, we monitored the aggregation of the non-amyloidogenic rIAPP, and found no evidence of aggregation (Figure 1a), as shown earlier by Abedini et al. (2016).

Previous CD studies have reported a transition from monomeric, disordered hIAPP to β-sheet rich fibrils, as in Figure 1b (Ashburn & Lansbury Jr, 1993; Kellock et al., 2016). However, α-helical intermediates have also been reported during hIAPP amyloid formation before the transition to β-sheet (Abedini et al., 2016). We did not observe the distinctive α-helical spectrum during the transition from random coil to β-sheet in PBS. Our CD spectrum for the monomeric starting state may be consistent with a minor population of α-helix, but others have obtained much more pronounced helical spectra in the presence of, and/or after extended treatment with, helix-promoting alcohols, including Tris buffer, and fluorinated alcohols, such as HFIP (Abedini et al., 2016). The helix-promoting effect of Tris are evident by comparing the monomeric starting structure of hIAPP in Tris and PBS (Figure S2). The helical tendencies of hIAPP are supported by secondary chemical shifts determined by NMR in Tris buffer (Williamson & Miranker, 2007). In particular, upfield shifts of the Hα atoms were observed relative to 'random coil' chemical shifts. Upfield shifts are taken as evidence of α-helical structure while downfield shifts are indicative of β-sheet (Wishart, 2011). However, similar Hα shifts are also observed for α-sheet structure: an "α-helical Chemical Shift Index" is obtained for the α_L-α_R-α_L-α_R-α_L-α_R-α_L stretches of the designed α-sheet peptide AP407, but α-helical structure is not present by NMR, CD, or IR (Shea et al., 2019). In the case of hIAPP, the presumed helical structure could be due to Tris or α-sheet structure. While alcohols and other organic solvents can promote helical structure, including nonnative helical structure, they can also help to elucidate helical propensities that may be biologically relevant (Cao et al., 2013; Williamson & Miranker, 2007).

There has been much discussion of toxic oligomers in hIAPP aggregation (Butler et al., 2003; Gurlo et al., 2010; Janson et al., 1999; Lin et al., 2007; Ritzel et al., 2007; Zraika et al., 2010). In this study, we found that oligomeric non-β-sheet hIAPP conformers were the most toxic species during aggregation and hIAPP fibrils were non-toxic. Notably, the increase in toxicity during the lag phase of aggregation corresponds to the formation of α-sheet (as shown by CD, and note the close correspondence to the AP407 CD spectrum) prior to β-structure formation. In addition, as hIAPP entered the early sigmoidal phase, toxicity decreased and was close to negligible at the plateau, coinciding with β-sheet formation. These results show a correlation between the formation of α-sheet structure and toxicity, which has also been observed for the β-amyloid peptide (Aβ42) associated with Alzheimer's Disease (Shea et al., 2019).

Our de novo synthetic α-sheet hairpin peptides designed to be complementary to the α-sheet structure in hIAPP toxic oligomers inhibited amyloid aggregation and neutralized toxicity while a random coil control peptide did not. This has also been observed for Aβ42 (Shea et al., 2019), PSMα1, the main component of amyloid fibrils in *Staphylococcus aureus* biofilms (Bleem et al., 2017), and CsgA, which is the main component of *E. coli* curli amyloid fibrils (Bleem et al., 2023). Aβ42 and CsgA undergo random coil → α-sheet → β-sheet transitions, like hIAPP, whereas PSMα1 converts from α-helix → α-sheet → β-sheet. α-Sheet designs also inhibit aggregation and toxicity of Aβ42, CsgA, and PSMα1 through selective binding of α-sheet oligomers, suggesting a conserved pathway of amyloid aggregation and toxicity pathway mediated by this nonstandard secondary structure. Our α-sheet designs have a novel mechanism of action via selective binding of the α-sheet structure in the toxic amyloidogenic oligomers, leading to a drop in both toxicity and amyloid burden.

While our results show that designed α-sheet peptides inhibit hIAPP toxicity in a cell-based assay, peptide access to hIAPP aggregates in intact islets was anticipated to be more difficult. To determine whether α-sheet peptides decrease endogenous islet amyloid formation, we evaluated the effect of α-sheet designs on islets isolated from hIAPP transgenic mice that express amyloidogenic hIAPP in the β-cell and are prone to develop amyloid. These isolated islets were cultured under amyloid-inducing conditions (Aston-Mourney et al., 2011; Templin et al., 2017; Zraika et al., 2007) in the presence or absence of AP5 or AP90. Treatment of hIAPP transgenic mouse islets with α-sheet peptides under amyloid-forming conditions (16.7 mM glucose) allowed us to study the effect of these peptides on endogenous islet amyloid formation in a model more closely related to the amyloid-induced β-cell loss observed in T2D. As previously observed using this model, significant amyloid deposition occurred in these hIAPP-expressing islets when cultured in 16.7 mM glucose (Hull et al., 2005). Administration of AP90 led to a reduction in endogenous islet amyloid formation, supporting our in vitro inhibition data (Figure 2a), and demonstrating that our compounds reduce islet amyloid deposition in situ. Coincident with this effect, we also observed an increase in β-cell area when hIAPP islets were treated with AP90 (Figure 6d). These findings support our in vitro cell viability results (Figure 2b) and reinforce the hypothesis that hIAPP α-sheet oligomers formed during the early phases of amyloid aggregation are associated with β-cell toxicity.

Importantly, as we anticipate further in vivo studies, we also found that AP90 neither made wild-type mice ill nor elicited an immune response over the course of 4 weeks of continuous peptide treatment.

4 | CONCLUSIONS

The results presented here demonstrate that α-sheet structure was populated in the lag phase of aggregation of hIAPP and is correlated with toxicity. The administration of complementary synthetic α-sheet peptides inhibited hIAPP toxicity and amyloid formation in vitro in INS-1 β-cells and neuroblastoma cells as well as in an hIAPP transgenic mouse model of islet amyloidosis. Moreover, these de novo synthetic α-sheet peptides did not appear to be toxic or trigger an immune reaction in mice. While much remains to be done, a better understanding of hIAPP aggregation and the role of α-sheet structure in amyloid-associated β-cell loss may provide a new strategy to combat the β-cell loss observed in humans with T2D by directly targeting toxic oligomeric hIAPP species while maintaining the native biological activity of hIAPP monomers.

5 | METHODS

5.1 | Preparation of human islet amyloid polypeptide

hIAPP (with amidated C-terminus and Cys2-Cys7 disulfide bond, Ontores Biotechnologies) was monomerized and aliquoted as described previously (Kellock et al., 2016). Aliquots were re-treated with HFIP and sonicated to remove any seeds, dried under nitrogen gas, and exsiccated in a SpeedVac concentrator (Savant). The aliquots were reconstituted in (a) dimethyl sulfoxide (DMSO, Sigma-Aldrich) and PBS buffer, and (b) ice-cold PBS. For method (a), aliquots were dissolved in DMSO followed by sonication and microcentrifugation. The final hIAPP concentrations were nominal, as DMSO interferes with UV absorbance. For method (b), aliquots were dissolved in ice-cold PBS buffer, sonicated in an ice-chilled water bath and used immediately. The stock concentration was measured with a NanoDrop UV–Vis spectrophotometer (ThermoScientific) at 280 nm.

5.2 | Synthesis of designed α-sheet peptides

Designed α-sheet and control peptides were synthesized and purified as described previously (Maris et al., 2018). The mass and peptide sequence of high-performance liquid chromatography (HPLC)—purified peptides were verified by mass spectrometry (MS; Bruker Daltonics).

5.3 | Thioflavin T (ThT) aggregation assay

Aggregation of hIAPP was tracked using a ThT (Sigma–Aldrich) assay with continuous or "undisturbed" methods to address the extra agitation introduced by the robotic movement of the plate reader (Sebastiao et al., 2017). For the 'undisturbed' method, hIAPP aggregated in a LoBind tube from which aliquots were removed and the fluorescence measured. For the continuous method, ThT binding was tracked directly in the microarray plate. For inhibition experiments, hIAPP was incubated with and without various peptides. Fluorescence was monitored on a multimode plate reader with excitation at 438 nm and emission monitored at 495 nm, measurement height 7.5 mm, 8 flashes (Perkin Elmer, Inspire).

5.4 | MTT cell viability assay

Cell viability, as a surrogate for cytotoxicity, was determined using the 3-(4,5-dimethylthiazol-2-yl)-2,5-diphenyltetrazolium bromide (MTT) assay in two cell lines. INS-1832/13 cells (University of Washington Diabetes Research Center) were cultured in RPMI-1640 (Gibco) medium supplemented with 10% fetal bovine serum (Invitrogen), 1 mM sodium pyruvate (Invitrogen), and 100 U/mL penicillin–streptomycin (Gibco).

SH-SY5Y cells (ATCC) were cultured in DMEM/F12 (Gibco) medium supplemented with 10% fetal bovine serum (Invitrogen), and 100 U/mL penicillin–streptomycin (Gibco), as previously described (Shea et al., 2019). The INS-1 and SH-SY5Y experiments are not comparable; they utilized different optimized conditions, including different toxic oligomer concentrations based on the behavior and tolerance of the cells. For example, the SH-SY5Y cells are more resistant to toxic oligomers than the INS-1 cells, so higher concentrations were necessary.

The INS-1 cells were seeded in a 96-well plate at 4×10^4 cells per well and the SH-SY5Y cells were plated at 10^5 cells per well. Cells were cultured in a CO_2 water-jacketed incubator (37°C, 5% CO_2; Forma Scientific) for 24 h, followed by addition of various treatments. Cells were cultured with treatments for 24 h before addition of MTT (5 mg/mL in PBS; Sigma) and then incubated for an additional 4 h. Lysis buffer (20% SDS, 50% DMF, 1% glacial acetic acid, and 0.2% HCl) was added to

each well and cells were incubated overnight at 25°C in the dark. The absorbance was measured at 570 nm.

5.5 | Circular dichroism spectroscopy

The CD spectra were collected on a Jasco J-720 spectrophotometer (Easton, MD) with a closed-top 10-mm-pathlength cuvette. IAPP was incubated at different concentrations, as noted above, but all samples were diluted with DI water to 15 μM for evaluation by CD. The CD spectra were smoothed with a 15-polynomial order Savitsky-Golay smoothing (Greenfield, 2006) and Fast Fourier Transform algorithm (Bush, 1974). The smoothed data were blanked and zeroed before converting to mean residue ellipticity (MRE).

5.6 | Soluble oligomer binding assay

The soluble oligomer-binding assay (SOBA) was used as described previously with the AP193 peptide used as the capture agent (sequence provided in Table S1) (Bi & Daggett, 2018; Shea et al., 2019), with the exception that an anti-hIAPP antibody (Abcam, diluted 1:5000) was substituted for the anti-Amyloid-β antibody. A goat secondary anti-rabbit HRP-conjugated antibody (Pierce, diluted 1:10,000) and Ultra TMB developing reagent (ThermoFisher) were employed.

5.7 | hIAPP transgenic mice

hIAPP transgenic mice on a C57BL/6J background were bred with DBA/2J mice obtained from Jackson Laboratories (Bar Harbor, ME, USA), and hemizygous hIAPP transgenic mice (F1 C57BL/6J × DBA/2J background) were studied with non-transgenic (wild type, WT) littermates as controls (Betsholtz et al., 1989; Hull et al., 2003; Verchere et al., 1996). The hIAPP transgene is expressed specifically in β-cells under the rat insulin II promoter. The study was reviewed and approved by the VA Puget Sound Health Care System Institutional Animal Care and Use Committee.

In the studies presented here, a total of 24 hIAPP transgenic and 9 WT mice were used.

5.8 | Islet isolation and treatment with α-sheet designs

Islets were isolated from 24 (8–12 week old) male and female mice by collagenase digestion. After overnight recovery, WT or hIAPP transgenic islets were cultured for 144 h in media containing 16.7 mM glucose, a condition resulting in amyloid formation in transgenic islets (Hull et al., 2005). Islets were cultured in the absence or presence of 100 μM α-sheet peptide and media was changed every 48 h. On a given day, islets were isolated from 3 WT or 3 hIAPP mice. Islets from WT or hIAPP mice were then pooled and divided into a control group cultured without α-sheet peptide and peptide treatment groups cultured with AP5 or AP90 peptides. On a given day, these groups of islets were regarded as a biological replicate. On separate days, 3 biological replicates were performed for WT islet studies (9 mice) and 5 biological replicates were performed for hIAPP islet studies (15 mice).

5.9 | Fluorescein-labeled peptide experiments

Islets were isolated from 3 transgenic hIAPP mice and cultured, as described. Then they were exposed to fluorescein-labeled AP5 or AP90 for the final 48 h of the 144-h culture period. Peptides were incubated in FITC-labeling solution and gently mixed in the dark. The FITC-labeled peptide was then exchanged into PBS using a PD10 desalting column. Islets were transferred to medium lacking peptides before imaging at 488 nm by brightfield and confocal microscopy (Leica SP5, 10× magnification).

5.10 | Immunohistochemistry and quantitative microscopy

Islets were fixed in 10% (wt/vol) neutral-buffered formalin, embedded in agar and paraffin, then sectioned at 10 μm intervals and stained with thioflavin S to visualize amyloid deposits. Anti-insulin antibody (#I2018, Sigma, St. Louis, MO; 1:5000) and goat anti-mouse Cy3 (#115-165-146, Jackson ImmunoResearch; 1:250) were used to visualize β-cell area, and Hoechst 33258 to visualize nuclei. Islet, insulin, and thioflavin S-positive areas were quantified using morphometric analyses performed by individuals blinded to sample genotypes and culture conditions using an E800 Eclipse epifluorescence microscope and NIS Elements Software (Nikon USA) (Bush, 1974). For each replicate, the amyloid prevalence was defined as the proportion of islets per mouse containing amyloid, amyloid severity as (Σ amyloid area/Σ islet area) × 100% for all islets, and β-cell area as (Σ β-cell area/Σ islet area) × 100% for all islets. An average of 29 ± 4.5 (mean ± SEM) islets were quantified per condition and replicate for hIAPP islet studies.

5.11 | In vivo administration of α-sheet designs

Mini-osmotic pumps (ALZET, model 2004) were filled with saline or AP90 (100 μM and 1 mM) 48 h before implantation. The day prior, 6 hIAPP transgenic mice (~20-week-old) were weighed and plasma was collected from the saphenous vein via a heparinized hematocrit tube. Two mice were in each treatment group: saline, 100 μM, 1 mM AP90. Mice were anesthetized with isoflurane, and mini-pumps were implanted subcutaneously over the scapular region. Mice were monitored for three consecutive days following surgery. Blood samples were collected via the saphenous vein 1, 2, 3, and 4-weeks post-surgery. After 4 weeks, the mice were euthanized by sodium pentobarbital overdose, terminal blood samples were collected, and spleens were removed.

5.12 | Immunogenicity of α-sheet design in vivo

Peripheral blood mononuclear cells were isolated from mouse spleens by Ficoll density gradient centrifugation, grown in 96-well plates, and incubated with or without AP90, or concanavalin A. 3H-thymidine (1 mCi/well) was then added for 18 h, cells were lysed, and 3H-thymidine incorporation was determined by scintillation counting. The stimulation index (SI) was calculated as mean counts per minute (CPM) stimulated/unstimulated.

5.13 | Mass spectrometry-based detection of α-sheet peptide in mouse plasma

AP90 was detected in mouse plasma using C18 tip exchange (Thermo Pierce C18 tips, 100 μL bed). 100 μL plasma was adjusted to 0.25% TFA. The C18 tip was primed twice with 100 μL of 50% ACN in water. The tip was then equilibrated twice with 100 μL of 0.1% TFA. Sample was then aspirated into the C18 tip, dispensed, and aspirated for a total of 10 cycles. The tip was rinsed twice with 100 μL of 0.1% TFA/5% ACN, and the sample was eluted for LC–MS analysis with 100 μL of 0.1% acetic acid in 70% ACN brought to 500 μL in 70/30 A/B (0.05% TFA/90% ACN 0.043% TFA) and dispensed into an auto sample vial. A 27.5 min gradient of 10–60% B at a flow of 1 μL/min over an analytical C18 HPLC column was used to identify AP90 peptide with the expected +2 and +3 peaks for undigested AP90—1412 m/z and 942 m/z, respectively.

5.14 | Statistical analysis

Data are reported as means ± standard deviation. Statistical differences were determined using the Student *t*-test or Mann–Whitney *U* test for nonparametric data. One-way ANOVA with Tukey multiple comparison corrections was used for data with more than two groups. A p-value <0.05 was considered statistically significant.

ACKNOWLEDGMENTS

INS-1 cells were provided by the University of Washington Diabetes Research Center. We thank Daryl Hackney of the Metabolism Group at the VA Puget Sound Health Care System for technical expertise. This research was supported by NIH Grant GMS 95808 (to V.-D.), University of Washington Office of Research and Department of Bioengineering (to V.D.), NIH Grant F32-DK-107022 (to A.T.T.), Department of Veterans Affairs Merit Review I01-BX001060 (to S.E.K.), American Diabetes Association Mentor-Based Fellowship 7-11-MN-28 (to S.E.K) and NIH Grant P30-DK-017047 that supports the Diabetes Research Center at the University of Washington. Student support was provided by a UW Mary Gates Research Scholarship (to C.H.) and the National Institute of Health Bioengineering and Cardiovascular Training Grant (NIH/NIBIB 532EB1650 to D.S., M. Regnier, P.I.) and Molecular Biophysics Training Grant (NIH/GMS T32GM008268 to T.P, N. Zheng, P.I.).

CONFLICT OF INTEREST STATEMENT

The authors declare that there are no competing interests.

DATA AVAILABILITY STATEMENT

The data that support the findings of this study are available from the corresponding authors upon reasonable request.

REFERENCES

Abedini A, Plesner A, Cao P, Ridgway Z, Zhang J, Tu LH, et al. Time-resolved studies define the nature of toxic IAPP intermediates, providing insight for anti-amyloidosis therapeutics. Elife. 2016;5:e12977.

Armen RS, Alonso DO, Daggett V. Anatomy of an amyloidogenic intermediate: conversion of β-sheet to α-sheet structure in transthyretin at acidic pH. Structure. 2004;12:1847–63.

Armen RS, DeMarco ML, Alonso DO, Daggett V. Pauling and Corey's α-pleated sheet structure may define the prefibrillar amyloidogenic intermediate in amyloid disease. Proc Natl Acad Sci U S A. 2004;101:11622–7.

Ashburn TT, Lansbury PT Jr. Interspecies sequence variations affect the kinetics and thermodynamics of amyloid formation: peptide models of pancreatic amyloid. J Am Chem Soc. 1993; 115:11012–3.

Aston-Mourney K, Hull RL, Zraika S, Udayasankar J, Subramanian SL, Kahn SE. Exendin-4 increases islet amyloid deposition but offsets the resultant β-cell toxicity in human islet amyloid polypeptide transgenic mouse islets. Diabetologia. 2011;54:1756–65.

Betsholtz C, Christmansson L, Engström U, Rorsman F, Svensson V, Johnson KH, et al. Sequence divergence in a specific region of islet amyloid polypeptide (IAPP) explains differences in islet amyloid formation between species. FEBS Lett. 1989;251:261–4.

Bi T, Daggett V. The role of α-sheet in amyloid oligomer aggregation and toxicity. Yale J Biol Med. 2018;91:247–55.

Bleem A, Francisco R, Bryers JD, Daggett V. Designed α-sheet peptides suppress amyloid formation in *Staphylococcus aureus* biofilms. NPJ Biofilms Microbiomes. 2017;3:16.

Bleem A, Prosswimmer T, Chen R, Hady TF, Li J, Bryers JD, et al. Designed α-sheet peptides disrupt uropathogenic *E. Coli* biofilm rendering bacteria susceptible to antibiotics and immune cells. Sci Rep. 2023;13:9272.

Brender JR, Krishnamoorthy J, Sciacca MF, Vivekanandan S, D'Urso L, Chen J, et al. Probing the sources of the apparent irreproducibility of amyloid formation: drastic changes in kinetics and a switch in mechanism due to micelle-like oligomer formation at critical concentrations of IAPP. J Phys Chem B. 2015;119:2886–96.

Bucciantini M, Giannoni E, Chiti F, Baroni F, Formigli L, Zurdo J, et al. Inherent toxicity of aggregates implies a common mechanism for protein misfolding diseases. Nature. 2002;416:507–11.

Bush CA. Fourier method for digital data smoothing in circular dichroism spectrometry. Anal Chem. 1974;46:3–8.

Butler AE, Janson J, Soeller WC, Butler PC. Increased β-cell apoptosis prevents adaptive increase in β-cell mass in mouse model of type 2 diabetes. Diabetes. 2003;52:2304–14.

Cao P, Marek P, Noor H, Patsalo V, Tu LH, Wang H, et al. Islet amyloid: from fundamental biophysics to mechanisms of cytotoxicity. FEBS Lett. 2013;587:1106–18.

Cao P, Meng F, Abedini A, Raleigh DP. The ability of rodent islet amyloid polypeptide to inhibit amyloid formation by human islet amyloid polypeptide has important implications for the mechanism of amyloid formation and the design of inhibitors. Biochemistry. 2010;49:872–81.

Cnop M, Vidal J, Hull RL, Utzschneider KM, Carr DB, Schraw T, et al. Progressive loss of β-cell function leads to worsening glucose tolerance in first-degree relatives of subjects with type 2 diabetes. Diabetes Care. 2007;30:677–82.

Cnop M, Welsh N, Jonas JC, Jorns A, Lenzen S, Eizirik DL. Mechanisms of pancreatic β-cell death in type 1 and type 2 diabetes: many differences, few similarities. Diabetes. 2005;54:S97–S107.

Cooper GJ, Willis AC, Clark A, Turner RC, Sim RB, Reid KB. Purification and characterization of a peptide from amyloid-rich pancreases of type 2 diabetic patients. Proc Natl Acad Sci U S A. 1987;84:8628–32.

Daggett V. α-Sheet: the toxic conformer in amyloid diseases? Acc Chem Res. 2006;39:594–602.

De Carufel CA, Nguyen PT, Sahnouni S, Bourgault S. New insights into the roles of sulfated glycosaminoglycans in islet amyloid polypeptide amyloidogenesis and cytotoxicity. Biopolymers. 2013;100:645–55.

Federici M, Hribal M, Perego L, Ranalli M, Caradonna Z, Perego C, et al. High glucose causes apoptosis in cultured human pancreatic islets of Langerhans: a potential role for regulation of specific Bcl family genes toward an apoptotic cell death program. Diabetes. 2001;50:1290–301.

Forbes JM, Cooper ME. Mechanisms of diabetic complications. Physiol Rev. 2013;93:137–88.

Greenfield NJ. Using circular dichroism spectra to estimate protein secondary structure. Nat Protoc. 2006;1:2876–90.

Gurlo T, Ryazantsev S, Huang CJ, Yeh MW, Reber HA, Hines OJ, et al. Evidence for proteotoxicity in β cells in type 2 diabetes: toxic islet amyloid polypeptide oligomers form intracellularly in the secretory pathway. Am J Pathol. 2010;176:861–9.

Hopping G, Kellock J, Barnwal RP, Law P, Bryers J, Varani G, et al. Designed α-sheet peptides inhibit amyloid formation by targeting toxic oligomers. Elife. 2014;3:e01681.

Hull RL, Andrikopoulos S, Verchere CB, Vidal J, Wang F, Cnop M, et al. Increased dietary fat promotes islet amyloid formation and β-cell secretory dysfunction in a transgenic mouse model of islet amyloid. Diabetes. 2003;52:372–9.

Hull RL, Shen ZP, Watts MR, Kodama K, Carr DB, Utzschneider KM, et al. Long-term treatment with rosiglitazone and metformin reduces the extent of, but does not prevent, islet amyloid deposition in mice expressing the gene for human islet amyloid polypeptide. Diabetes. 2005;54:2235–44.

Hull RL, Westermark GT, Westermark P, Kahn SE. Islet amyloid: a critical entity in the pathogenesis of type 2 diabetes. J Clin Endocrinol Metab. 2004;89:3629–43.

Janson J, Ashley RH, Harrison D, McIntyre S, Butler PC. The mechanism of islet amyloid polypeptide toxicity is membrane disruption by intermediate-sized toxic amyloid particles. Diabetes. 1999;48:491–8.

Kahn SE, D'Alessio DA, Schwartz MW, Fujimoto WY, Ensinck JW, Taborsky GJ Jr, et al. Evidence of cosecretion of islet amyloid polypeptide and insulin by β-cells. Diabetes. 1990;39:634–8.

Kahn SE, Hull RL, Utzschneider KM. Mechanisms linking obesity to insulin resistance and type 2 diabetes. Nature. 2006;444:840–6.

Kayed R, Head E, Thompson JL, McIntire TM, Milton SC, Cotman CW, et al. Common structure of soluble amyloid oligomers implies common mechanism of pathogenesis. Science. 2003;300:486–9.

Kellock J, Hopping G, Caughey B, Daggett V. Peptides composed of alternating L- and D-amino acids inhibit amyloidogenesis in three distinct amyloid systems independent of sequence. J Mol Biol. 2016;428:2317–28.

Kharroubi I, Ladrière L, Cardozo AK, Dogusan Z, Cnop M, Eizirik DL. Free fatty acids and cytokines induce pancreatic β-cell apoptosis by different mechanisms: role of nuclear factor-κB and endoplasmic reticulum stress. Endocrinology. 2004;145:5087–96.

Kim J, Park K, Kim MJ, Lim H, Kim KH, Kim SW, et al. An autophagy enhancer ameliorates diabetes of human *IAPP*-transgenic mice through clearance of amyloidogenic oligomer. Nat Commun. 2021;12:183.

Lin CY, Gurlo T, Kayed R, Butler AE, Haataja L, Glabe CG, et al. Toxic human islet amyloid polypeptide (h-IAPP) oligomers are intracellular, and vaccination to induce anti-toxic oligomer antibodies does not prevent h-IAPP-induced β-cell apoptosis in h-IAPP transgenic mice. Diabetes. 2007;56:1324–32.

Linse S. Monomer-dependent secondary nucleation in amyloid formation. Biophys Rev. 2017;9:329–38.

Maris NL, Shea D, Bleem A, Bryers JD, Daggett V. Chemical and physical variability in structural isomers of an L/D α-sheet peptide designed to inhibit Amyloidogenesis. Biochemistry. 2018; 57:507–10.

Meier JJ, Kayed R, Lin CY, Gurlo T, Haataja L, Jayasinghe S, et al. Inhibition of human IAPP fibril formation does not prevent β-cell death: evidence for distinct actions of oligomers and fibrils of human IAPP. AJP Endocrinol Metab. 2006;291: E1317–24.

Oskarsson ME, Hermansson E, Wang Y, Welsh N, Presto J, Johansson J, et al. BRICHOS domain of Bri2 inhibits islet amyloid polypeptide (IAPP) fibril formation and toxicity in human β-cells. Proc Natl Acad Sci U S A. 2018;115: E2752–61.

Prosswimmer T, Daggett V. The role of α-sheet structure in amyloidogenesis: characterization and implications. Open Biol. 2022; 12(11):220261. https://doi.org/10.1098/rsob.220261.

Ritzel RA, Meier JJ, Lin CY, Veldhuis JD, Butler PC. Human islet amyloid polypeptide oligomers disrupt cell coupling, induce apoptosis, and impair insulin secretion in isolated human islets. Diabetes. 2007;56:65–71.

Saeedi P, Petersohn I, Salpea P, Malanda B, Karuranga S, Unwin N, et al. Global and regional diabetes prevalence estimates for 2019 and projections for 2030 and 2045: results from the international diabetes federation diabetes atlas. Diabetes Res Clin Pract. 2019;157:107843.

Sebastiao M, Quittot N, Bourgault S. Thioflavin T fluorescence to analyse amyloid formation kinetics: measurement frequency as a factor explaining irreproducibility. Anal Biochem. 2017;532: 83–6.

Shea D, Colasurdo E, Smith A, Paschall C, Jayadev S, Keene CD, et al. SOBA: development and testing of a soluble oligomer binding assay for detection of amyloidogenic toxic oligomers. Proc Natl Acad Sci U S A. 2022;119:e2213157119.

Shea D, Hsu CC, Bi TM, Paranjapye N, Childers MC, Cochran J, et al. α-Sheet secondary structure in amyloid β-peptide drives aggregation and toxicity in Alzheimer's disease. Proc Natl Acad Sci U S A. 2019;116:8895–900.

Shigihara N, Fukunaka A, Hara A, Komiya K, Honda A, Uchida T, et al. Human IAPP-induced pancreatic β cell toxicity and its regulation by autophagy. J Clin Invest. 2014;124:3634–44.

Templin AT, Samarasekera T, Meier DT, Hogan MF, Mellati M, Crow MT, et al. Apoptosis repressor with caspase recruitment domain ameliorates amyloid-induced ß-cell apoptosis and JNK pathway activation. Diabetes. 2017;66:2636–45.

Verchere CB, D'Alessio DA, Palmiter RD, Weir GC, Bonner-Weir S, Baskin DG, et al. Islet amyloid formation associated with hyperglycemia in transgenic mice with pancreatic β-cell expression of human islet amyloid polypeptide. Proc Natl Acad Sci U S A. 1996;93:3492–6.

Westermark P, Wernstedt C, Wilander E, Hayden DW, O'Brien TD, Johnson KH. Amyloid fibrils in human insulinoma and islets of Langerhans of the diabetic cat are derived from a neuropeptide-like protein also present in normal islet cells. Proc Natl Acad Sci U S A. 1987;84:3881–5.

Williamson JA, Miranker AD. Direct detection of transient α-helical states in islet amyloid polypeptide. Prot Sci. 2007;16:110–7.

Wishart D. Interpreting protein chemical shift data. Prog Nucl Magn Reson Spectrosc. 2011;58:62–87.

Zraika S, Hull RL, Udayasankar J, Utzschneider KM, Tong J, Gerchman F, et al. Glucose and time-dependence of islet amyloid formation in vitro. Biochem Biophys Res Commun. 2007; 354:234–9.

Zraika S, Hull RL, Verchere CB, Clark A, Potter KJ, Fraser PE, et al. Toxic oligomers and islet β-cell death: guilty by association or convicted by circumstantial evidence? Diabetologia. 2010;53:1046–56.

SUPPORTING INFORMATION

Additional supporting information can be found online in the Supporting Information section at the end of this article.

How to cite this article: Hsu C-C, Templin AT, Prosswimmer T, Shea D, Li J, Brooks-Worrell B, et al. Human islet amyloid polypeptide-induced β-cell cytotoxicity is linked to formation of α-sheet structure. Protein Science. 2024;33(2):e4854. https://doi.org/10.1002/pro.4854